The Journal of Chemical Physics

Constrained nuclear-electronic orbital density functional theory: Energy surfaces with nuclear quantum effects

Cite as: J. Chem. Phys. **152**, 084107 (2020); https://doi.org/10.1063/1.5143371
Submitted: 23 December 2019 . Accepted: 09 February 2020 . Published Online: 26 February 2020

Xi Xu, and Yang Yang

The Journal of Chemical Physics ARTICLE scitation.org/journal/jcp

Constrained nuclear-electronic orbital density functional theory: Energy surfaces with nuclear quantum effects

Cite as: J. Chem. Phys. 152, 084107 (2020); doi: 10.1063/1.5143371
Submitted: 23 December 2019 • Accepted: 9 February 2020 •
Published Online: 26 February 2020

Xi Xu and Yang Yang[a)]

AFFILIATIONS

Department of Chemistry and Theoretical Chemistry Institute, University of Wisconsin-Madison, 1101 University Avenue, Madison, Wisconsin 53706, USA

[a)]Author to whom correspondence should be addressed: yyang222@wisc.edu

ABSTRACT

The nuclear-electronic orbital (NEO) framework enables the incorporation of nuclear quantum effects by treating both electrons and specific key nuclei quantum-mechanically. The conventional NEO method predicates on the controversial Born–Oppenheimer separation between classical and quantum nuclei, and its potential energy surface only depends on the coordinates of classical nuclei. In this paper, based on the fact that quantum nuclei are relatively localized, we develop the constrained nuclear-electronic orbital density functional theory (cNEO-DFT) by imposing a constraint on the expectation value of the quantum nuclear position. In this way, an extended NEO energy surface is obtained, which also depends on the quantum nuclear position. Compared to the potential energy surface obtained from conventional DFT, the extended NEO energy surface incorporates the nuclear quantum effects, which have notable impacts on the energy profile. Furthermore, cNEO-DFT can facilitate the location of NEO stationary states. It potentially can be used in geometry optimization, transition states search, and the calculation of reaction dynamics.

I. INTRODUCTION

Nuclear quantum effects, such as zero-point energy and hydrogen tunneling, can be crucial in the description of many chemical and biological systems. Typical examples are the proton-coupled electron transfer (PCET) reactions[1] in fuel cells,[2] electrochemical devices,[3,4] photosynthesis, and respiration.[5,6] The nuclear-electronic orbital (NEO) approach,[7–10] which treats both electrons and specific nuclei quantum-mechanically within the orbital picture, has been developed to describe the nuclear quantum effects. Similar to the conventional electronic structure theory, NEO also includes both wave-function methods and density functional theory (NEO-DFT). The wave-function methods, such as NEO Hartree–Fock[7,8] (NEO-HF) and NEO coupled-cluster theory[11,12] (NEO-CC), can be systematically improved but are usually more computationally expensive. In contrast, NEO-DFT is more computationally feasible, while the challenge often lies in the development of a good electron–proton correlation (EPC) functional.[13–17] In the past decade, there have been many achievements in the NEO field, ranging from method development to preliminary applications in simple systems, and from the calculation of ground state properties[18,19] to the prediction of vibrational excited states.[20–22]

Despite these great achievements, all previous NEO developments rely on the assumption that quantum nuclei and electrons will respond instantaneously to the motion of classical nuclei.[23] Under this assumption, the orbitals of the quantum nuclei and all the electrons are optimized to stationary solutions, which depend on the positions of classical nuclei. Consequently, the NEO potential energy surface is only a function of classical nuclear positions.[23] This is the Born–Oppenheimer separation in the NEO framework. Unfortunately, because of the relatively small mass difference between the quantum and classical nuclei, this separation is considered less physical than the conventional Born–Oppenheimer separation between electrons and nuclei. As a result, neither the vibrational excitations calculated from NEO time-dependent density functional theory[20] (NEO-TDDFT) nor the normal modes obtained from the

diagonalization of the NEO Hessian matrix[23] correspond to the vibrations observed in experiments.[21,24] Although a special approach that combines NEO-TDDFT and NEO Hessian has been developed to recover the real vibrations, it is not perfect with the anharmonic effects included in a harmonic treatment.[21] In this paper, we develop the constrained nuclear-electronic orbital density functional theory (cNEO-DFT) to overcome the problems related to the unphysical NEO Born–Oppenheimer separation. By imposing a constraint on the expectation value of the quantum nuclear position operator, we obtain an extended NEO energy surface as a function of the expectation position of the quantum nuclei as well as the position of the classical nuclei. In the way, the assumption that the quantum nuclei respond immediately to the motion of classical nuclei is not invoked. Furthermore, the extended surface naturally incorporates nuclear quantum effects, which have a notable impact on the energy profile.

This paper is organized as follows: The derivation of cNEO-DFT, which is performed analogously to the constrained density functional theory,[25–27] is presented in Sec. II. Then, the energy surfaces of the three model systems, FHF^-, HCN/HNC isomerization, and hydrogen transfer in 2-cyano-malondialdehyde, are investigated by cNEO-DFT, and the computational details and results are presented in Sec. III and Sec. IV, respectively. The results are also compared to the potential energy surfaces obtained by conventional DFT to investigate the impacts of nuclear quantum effects. Finally, our concluding remarks are provided in Sec. V.

II. THEORY

In the NEO framework, both electrons and specific key nuclei are treated quantum mechanically. For simplicity, we only consider quantum protons in this paper, but the theory can be easily extended to other types of quantum nuclei.

In NEO-DFT,[9] the non-interacting Kohn–Sham reference is the product of an electronic determinant and a proton determinant,

$$|\Psi\rangle = |\Psi^e\rangle|\Psi^p\rangle. \tag{1}$$

The superscripts e and p refer to electrons and protons, respectively. The total energy can be expressed as a functional of both electron and proton densities,

$$\begin{aligned} E[\rho^e,\rho^p] = &(T_s[\rho^e] + T_s[\rho^p]) + (J^{ee}[\rho^e] + J^{pp}[\rho^p] + J^{ep}[\rho^e,\rho^p]) \\ &+ (E^e_{xc}[\rho^e] + E^p_{xc}[\rho^p]) + (E^{ep}_c[\rho^e,\rho^p]) \\ &+ (E^e_{ext}[\rho^e] + E^p_{ext}[\rho^p]), \end{aligned} \tag{2}$$

where the quantities in each parenthesis represent the kinetic energy of the non-interacting reference, mean-field Coulomb interaction energy, same-particle exchange-correlation energy, electron–proton correlation energy, and external potential energy, respectively. The electron and proton densities are defined in terms of occupied orbitals,

$$\rho^e = \sum_i^{N^e} |\phi^e_i|^2, \tag{3}$$

$$\rho^p = \sum_I^{N^p} |\phi^p_I|^2, \tag{4}$$

where N^e is the number of electrons and N^p is the number of protons. We use lowercase i and uppercase I to index the occupied electron orbitals and occupied proton orbitals, respectively.

Minimizing the energy functional E by varying electron and proton orbitals under the orbital normalization constraints leads to the conventional NEO-DFT eigenvalue equations,

$$\left(-\frac{1}{2}\nabla^2 + v^e\right)\phi^e_i = \epsilon^e_i\phi^e_i, \tag{5}$$

$$\left(-\frac{1}{2}\nabla^2 + v^p\right)\phi^p_I = \epsilon^p_I\phi^p_I, \tag{6}$$

where the effective potentials for electrons and protons are defined as

$$v^e = v^{ee}_J + v^{pe}_J + v^e_{xc} + v^e_{epc} + v^e_{ext}, \tag{7}$$

$$v^p = v^{pp}_J + v^{ep}_J + v^p_{xc} + v^p_{epc} + v^p_{ext}. \tag{8}$$

Each term is obtained by taking the functional derivative of the corresponding energy term in Eq. (2) with respect to either electron or proton density.

In order to obtain the extended energy surface, here we introduce another constraint during the minimization, which is the expectation value of the quantum nuclear position. This is based on the fact that the protons are relatively localized, and at a given time, the expectation position of each proton can be perceived as its instantaneous position.[21] For simplicity, we restrict our discussion to a one-proton case in this paper, but the generalization to many-nuclei cases is straightforward and will be presented in future work.

The constraint imposed on the expectation value of the position for a single proton is

$$\mathbf{R_0} = \langle\Psi^p|\mathbf{r}|\Psi^p\rangle = \langle\phi^p|\mathbf{r}|\phi^p\rangle. \tag{9}$$

Here in the one-proton case, the proton determinant Ψ^p is simply the orbital function ϕ^p. Under this new constraint, the Lagrangian function can be written as

$$L = E + \mathbf{f}\cdot(\langle\phi^p|\mathbf{r}|\phi^p\rangle - \mathbf{R_0}) - \sum_i \epsilon^e_i(\langle\phi^e_i|\phi^e_i\rangle - 1) - \epsilon^p(\langle\phi^p|\phi^p\rangle - 1), \tag{10}$$

where $\mathbf{f}$ is the Lagrange multiplier introduced for the new constraint. Note that $\mathbf{f}$ is a vector because we are imposing the constraint in three dimensions, i.e., $\langle x\rangle = x_0$, $\langle y\rangle = y_0$, and $\langle z\rangle = z_0$. Making the Lagrangian function stationary with respect to orbital variations will lead to new coupled eigenvalue equations for electrons and the proton. Because the new constraint only acts on the density of the proton, the form of the electronic equation is the same as Eq. (5),

$$\left(-\frac{1}{2}\nabla^2 + v^e\right)\phi^e_i = \epsilon^e_i\phi^e_i, \tag{11}$$

in which the definition of v^e is the same as Eq. (7). In contrast, an extra term in the proton equation shows up due to the new constraint,

$$\left(-\frac{1}{2}\nabla^2 + v^p + \mathbf{f}\cdot\mathbf{r}\right)\phi^p_I = \epsilon^p_I\phi^p_I, \tag{12}$$

in which the definition of v^p is the same as Eq. (8). Note that although the form of the electronic equation remains the same, its solution does not because the electronic Fock operator depends on the proton density, which changes because of the new proton equation.

For a given Lagrange multiplier $\mathbf{f}$, it is straightforward to solve the coupled equations self-consistently and obtain a set of orbitals $\{\phi\} = \{\phi_i^e, \phi_I^p\}$ and orbital energies $\{\epsilon\} = \{\epsilon_i^e, \epsilon_I^p\}$. Therefore, all the orbitals and orbital energies are functions of the Lagrange multiplier $\mathbf{f}$,

$$\phi = \phi(\mathbf{f}), \tag{13}$$

$$\epsilon = \epsilon(\mathbf{f}). \tag{14}$$

However, for an arbitrary $\mathbf{f}$, the orbitals obtained would not necessarily satisfy the constraint in Eq. (9). Therefore, a proper $\mathbf{f}$, which leads to proton orbitals that satisfy the constraint, needs to be solved. In this paper, we use the following way to solve the proper $\mathbf{f}$.

When the new coupled equations [Eqs. (11) and (12)] are solved with a given $\mathbf{f}$, L is stationary with respect to any orbital variation

$$\frac{\delta L}{\delta \phi} = \frac{\delta L}{\delta \phi^*} = 0. \tag{15}$$

Its derivatives with respect to orbital energies are also 0,

$$\frac{\partial L}{\partial \epsilon} = \langle \phi | \phi \rangle - 1 = 0. \tag{16}$$

Because orbitals and orbital energies are both functions of $\mathbf{f}$, the total derivative of L with respect to $\mathbf{f}$ is

$$\begin{aligned}\frac{\mathrm{d}L}{\mathrm{d}\mathbf{f}} &= \frac{\partial L}{\partial \mathbf{f}} + \left(\sum_{\phi} \int \frac{\delta L}{\delta \phi(\mathbf{r})} \frac{\mathrm{d}\phi(\mathbf{r})}{\mathrm{d}\mathbf{f}} \mathrm{d}\mathbf{r} + \sum_{\phi^*} \int \frac{\delta L}{\delta \phi^*(\mathbf{r})} \frac{\mathrm{d}\phi^*(\mathbf{r})}{\mathrm{d}\mathbf{f}} \mathrm{d}\mathbf{r} \right) \\ &\quad + \sum_{\epsilon} \frac{\partial L}{\partial \epsilon} \frac{\mathrm{d}\epsilon}{\mathrm{d}\mathbf{f}} \\ &= \frac{\partial L}{\partial \mathbf{f}} = \langle \phi^p | \mathbf{r} | \phi^p \rangle - \mathbf{R}_0. \end{aligned} \tag{17}$$

This equation holds true for any $\mathbf{f}$. At the proper $\mathbf{f}$, the corresponding orbitals satisfy the constraint in Eq. (9). Then, this total derivative vanishes, which indicates that the Lagrangian function L reaches an extremum with respect to the change in $\mathbf{f}$. Therefore, solving the proper $\mathbf{f}$ is equivalent to solving the equation

$$\frac{\mathrm{d}L(\mathbf{f})}{\mathrm{d}\mathbf{f}} = \langle \phi^p(\mathbf{f}) | \mathbf{r} | \phi^p(\mathbf{f}) \rangle - \mathbf{R}_0 = 0. \tag{18}$$

Many numerical algorithms, such as the Krylov algorithm[28] and the Anderson algorithm,[29] can be employed to find the solution. Alternatively, the non-degenerate perturbation theory can be used to evaluate the second-order derivative of L with respect to $\mathbf{f}$, and then the Newton's method can be utilized to find the solution iteratively. The second-order derivative of L with respect to $\mathbf{f}$ is

$$\begin{aligned}\frac{\mathrm{d}^2 L}{\mathrm{d}\mathbf{f}^2} &= \frac{\mathrm{d}}{\mathrm{d}\mathbf{f}} \Bigg(\langle \phi^p | \mathbf{r} | \phi^p \rangle - \mathbf{R}_0 + \sum_{\phi} \int \frac{\delta L}{\delta \phi(\mathbf{r})} \frac{\mathrm{d}\phi(\mathbf{r})}{\mathrm{d}\mathbf{f}} \mathrm{d}\mathbf{r} \\ &\quad + \sum_{\phi^*} \int \frac{\delta L}{\delta \phi^*(\mathbf{r})} \frac{\mathrm{d}\phi^*(\mathbf{r})}{\mathrm{d}\mathbf{f}} \mathrm{d}\mathbf{r} + \sum_{\epsilon} \frac{\partial L}{\partial \epsilon} \frac{\mathrm{d}\epsilon}{\mathrm{d}\mathbf{f}} \Bigg) \\ &= \left\langle \frac{\mathrm{d}\phi^p}{\mathrm{d}\mathbf{f}} | \mathbf{r} | \phi^p \right\rangle + \left\langle \phi^p | \mathbf{r} | \frac{\mathrm{d}\phi^p}{\mathrm{d}\mathbf{f}} \right\rangle. \end{aligned} \tag{19}$$

Note that because $\frac{\delta L}{\delta \phi(\mathbf{r})} = 0$ and $\frac{\partial L}{\partial \epsilon} = 0$ are always satisfied for any $\mathbf{f}$ after solving the coupled eigenvalue equations [Eqs. (11) and (12)], the derivatives with respect to $\mathbf{f}$ for the last three terms in the first line always vanish. The derivative of the proton orbital function with respect to the Lagrange multiplier can be calculated with the perturbation theory: when the term $\mathbf{f} \cdot \mathbf{r}$ is treated as an external perturbation in the proton equation [Eq. (12)], the first-order orbital change is

$$\phi^{p'} \approx \sum_A \frac{\langle \phi_A^p | \mathbf{f} \cdot \mathbf{r} | \phi^p \rangle}{\epsilon^p - \epsilon_A^p} \phi_A^p, \tag{20}$$

where the summation runs over all the virtual proton orbitals A. Note that this is an approximate expression because the screening effect is neglected.[30] In other words, the changes in the effective potential due to the change of orbitals are not counted in. Consequently, although this approximation generally leads to a robust algorithm, it may occasionally cause convergence problems. Under this approximation, the second-order derivative becomes

$$\frac{\mathrm{d}^2 L}{\mathrm{d}\mathbf{f}^2} \approx 2 \sum_A \frac{\langle \phi_A^p | \mathbf{r} | \phi^p \rangle \otimes \langle \phi^p | \mathbf{r} | \phi_A^p \rangle}{\epsilon^p - \epsilon_A^p}. \tag{21}$$

This expression is negative definite because the denominator is always negative and the numerator is positive definite.

With the assessment to the first and the second derivatives, Newton's iteration scheme to solve $\frac{\mathrm{d}L(\mathbf{f})}{\mathrm{d}\mathbf{f}} = 0$ becomes

$$\begin{aligned}\mathbf{f}^{n+1} &= \mathbf{f}^n - [L''(\mathbf{f}^n)]^{-1} L'(\mathbf{f}^n) \\ &= \mathbf{f}^n - \left[2 \sum_A \frac{\langle \phi_A^p | \mathbf{r} | \phi^p \rangle \otimes \langle \phi^p | \mathbf{r} | \phi_A^p \rangle}{\epsilon^p - \epsilon_A^p} \right]^{-1} [\langle \phi^p | \mathbf{r} | \phi^p \rangle - \mathbf{R}_0]. \end{aligned} \tag{22}$$

The iteration process stops when the first-order derivative approaches zero within a specified numerical precision.

Additionally, it can be proved that the negative of the Lagrange multiplier is the gradient of the total energy with respect to the expectation value of the proton expectation position $\mathbf{R}_0$, i.e., $-\mathbf{f} = \frac{\mathrm{d}E}{\mathrm{d}\mathbf{R}_0}$ (see the Appendix for detailed proof). Therefore, the Lagrange multiplier $\mathbf{f}$ is the internal force acting on the proton if the proton can be seen as a classical object.

III. COMPUTATIONAL DETAILS

We implemented the cNEO method in the PySCF package,[31] and all the subsequent calculations were performed with PySCF. We employed cNEO-DFT to calculate the energy surfaces for the hydrogen in three test cases: FHF^-, HCN/HNC isomerization, and hydrogen transfer in 2-cyano-malondialdehyde. The geometries of

these molecules were optimized by DFT/B3LYP[32–34] with the cc-pVTZ basis set[35] until the maximal force on every atom was less than 10^{-4} hartree/Å. In the latter two systems, all nuclei except the transferring hydrogen were fixed at the average reactant/product geometry. The coordinates of the geometries are presented in the supplementary material. In cNEO-DFT, the electronic exchange-correlation was described by the B3LYP functional, the single proton in the test systems was treated at the Hartree–Fock level, and no EPC functional was adopted in the calculations. Although it has been shown that EPC plays an important role in the accurate description of the nuclear quantum effects,[16,18] it is not the focus of the current paper, and its effects on cNEO-DFT will be investigated in future research. The cc-pVTZ basis for electrons and the 8*s*8*p*8*d* even-tempered Gaussian basis[36] ($\alpha = 2\sqrt{2}$, $\beta = \sqrt{2}$) for the quantum proton centered at the specified proton expectation position were used in all cNEO-DFT calculations. For comparison, the hydrogen potential energy surfaces by DFT/B3LYP were also calculated with the same electronic basis set at the same geometry. The only difference is that the proton was treated as a point charge in DFT, whereas it was delocalized with a specified expectation position in cNEO-DFT.

IV. RESULTS AND DISCUSSIONS

A. FHF^-

In FHF^-, the two F atoms are fixed at their equilibrium positions. Conventional NEO-DFT calculations can only get the stationary solution, where the proton density is centered between the two F atoms with the expectation position being the midpoint. In contrast, in cNEO-DFT, the expectation position for the proton can be specified at any point in the space, and, therefore, an energy surface that depends on the proton expectation position can be obtained, which is presented in Fig. 1(a). Note that when the expectation position is set to the midpoint of the two F atoms, the cNEO-DFT solution will coincide with the conventional NEO-DFT solution with a vanishing Lagrange multiplier **f**.

For comparison, the potential energy surface of FHF^- by DFT as a function of the hydrogen position is presented in Fig. 1(b). It is qualitatively similar to the energy surface by cNEO-DFT, but with a distinguishable quantitative difference. The cNEO-DFT predicts a higher absolute energy than the conventional DFT at any given molecular geometry, which is due to the inclusion of the proton kinetic energy in the delocalized proton orbital picture. The two energy surfaces are plotted with the same energy interval, and it can be observed that cNEO-DFT predicts a slightly shallower well than DFT along the y direction on the x = 0 axis. The reason is that although the proton kinetic energy is included throughout the whole space in cNEO-DFT, the relative magnitudes are different. When the proton is more localized near the bonding area, its kinetic energy is larger compared to the area far away with a more delocalized proton density. This suggests that the nuclear quantum effects incorporated by cNEO-DFT have discernible impacts on the energy landscape.

The Lagrange multiplier **f** for each proton expectation position is plotted in Fig. 1(c). As is proved in the Appendix, it serves as the force acting on the proton at a specified proton expectation position. This can also be intuitively verified by examining Figs. 1(a) and 1(c): the direction of **f** is consistent with the steepest descent direction in the energy landscape, and the length of the **f** vector is proportional

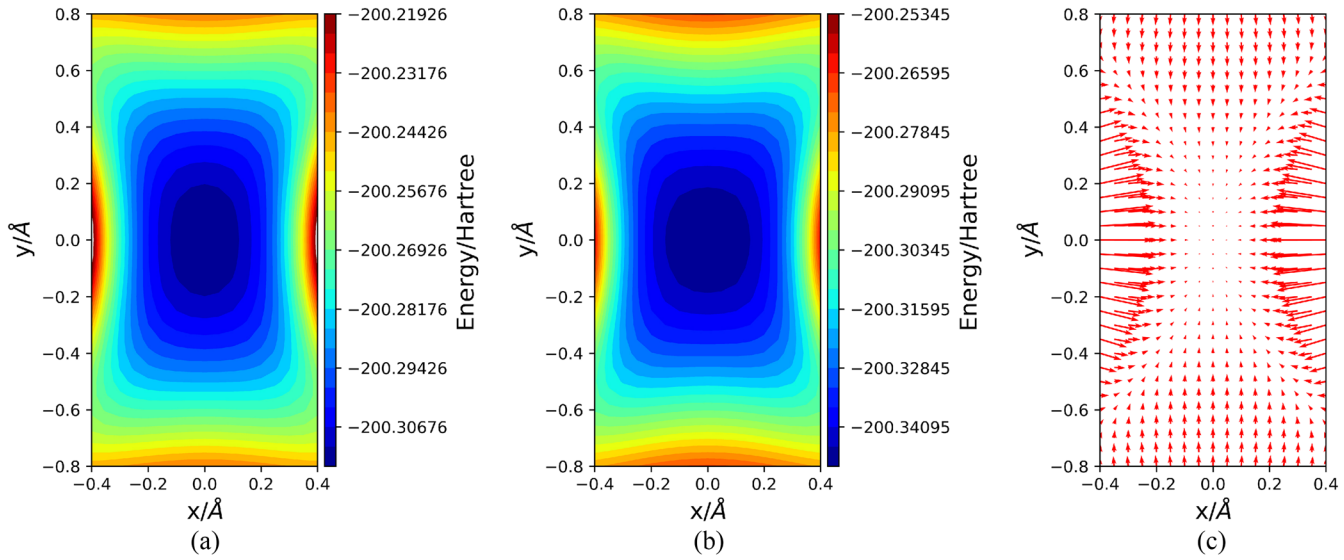

FIG. 1. Energy surfaces for the hydrogen atom in FHF^- by (a) cNEO-DFT and (b) conventional DFT. The two F atoms are positioned on the x-axis at 1.149 Å and −1.149 Å, respectively. Although the absolute energies are different, the energy intervals in (a) and (b) are set to be the same to facilitate the comparison. The hydrogen is in a single-well potential in both pictures, but the depths of the well are slightly different along the y direction on the x = 0 axis. The Lagrange multiplier **f** in cNEO-DFT at each proton expectation position is plotted in (c). The **f** vectors correspond to the negative of the energy gradient in (a) and serve as the force acting on the proton at each expectation position.

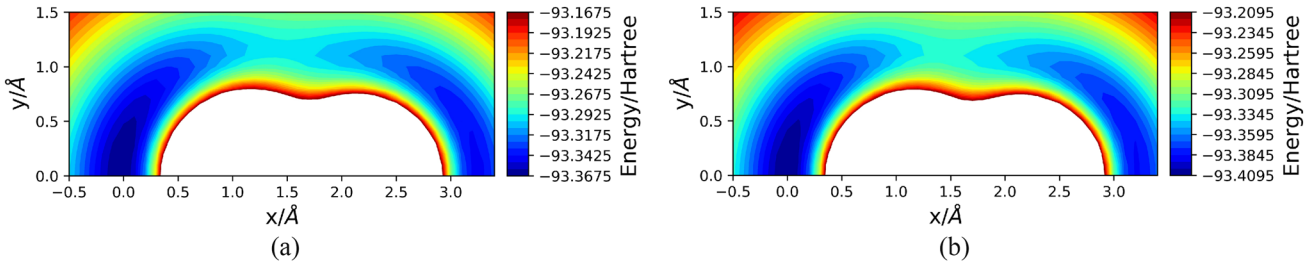

FIG. 2. Energy surfaces calculated by (a) cNEO-DFT and (b) DFT for the HCN/HNC isomerization. The C and N are fixed on the x axis at 1.064 Å and 2.220 Å, respectively. Although the absolute energies are different, the energy intervals in the plots are set to be the same to facilitate the comparison. The white color in the middle area indicates that the total energy is beyond the plotted energy range.

to the rate of the energy change in its direction. Note that **f** vanishes at the energy minimum when the proton is in the middle of the two F atoms, indicating a stable geometry with no internal force on the proton.

B. HCN/HNC isomerization

With fixed coordinates for the C and N atoms, the energy surfaces as a function of the proton (expectation) position for the HCN/HNC isomerization by cNEO-DFT and DFT are presented in Figs. 2(a) and 2(b), respectively. There are two local minima and one saddle point on the energy surfaces. The two local minima correspond to the HCN and HNC molecules, respectively, with the energy of HCN lower than that of HNC. The saddle point is the transition state for the HCN/HNC isomerization. Detailed plots around the saddle point by cNEO-DFT and DFT are presented in Figs. 3(a) and 3(b), respectively. The previous work on the stability of NEO-DFT solutions has located the two local minima by changing the initial guess in the NEO self-consistent-field (SCF) procedure but has not been able to locate the saddle point.[19] In our current development on cNEO-DFT, not only the two local minima, but also the saddle point can be easily identified by varying the proton expectation position. This is another strength of cNEO-DFT compared to conventional NEO-DFT. In addition, note that with the introduction of **f**, which serves both as an extra potential term in the proton eigenvalue equation [Eq. (12)] and as the force acting on the proton [Eq. (A3)], the stationary points in the NEO orbital space and the stationary points in the geometry space are connected.

By comparing the energy landscapes in the vicinity of the saddle point in Figs. 3(a) and 3(b), we can identify two major differences between the cNEO-DFT results and the conventional DFT results. First, at the corresponding saddle points, the proton is farther away from the C–N axis in cNEO-DFT than in conventional DFT. This can also be qualitatively understood by considering the relative magnitude of the proton kinetic energy at different proton expectation positions in cNEO-DFT. The farther the proton is, the more delocalized it is due to a flatter potential, and the lower the kinetic energy and the total energy are. The second difference is that the energy change along the reaction path described by cNEO-DFT is smaller than that of DFT, which is manifested by a smaller barrier in Figs. 2(a) and 3(a). This is also due to the more delocalized proton density near the saddle point compared to the minima. These two major differences suggest that the nuclear quantum effects have notable impacts on the geometry of the transition state as well as the whole reaction path.

The Lagrange multiplier **f** near the saddle point is shown in Fig. 3(c). Again, it corresponds to the force acting on the proton. The reaction path can also be clearly observed with those nearly vanishing arrows. Similar to the two minima, **f** also vanishes at the saddle point, but a tiny deviation along the reaction path will lead to a force that drives the proton away from the stationary position.

C. 2-cyano-malondialdehyde

2-cyano-malonaldehyde is another example of the intramolecular hydrogen transfer. This asymmetric molecule has also been investigated in previous NEO calculations with two local minima

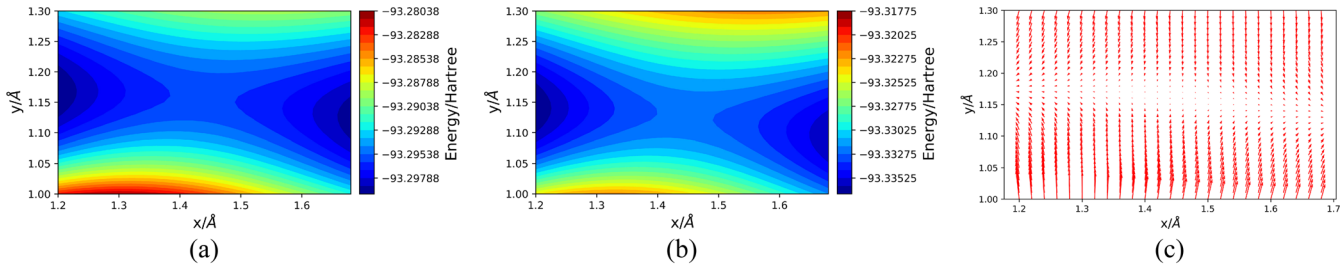

FIG. 3. A detailed plot of the energy surfaces around the saddle point for the HCN/HNC isomerization by (a) cNEO-DFT and (b) DFT, respectively. The Lagrange multiplier **f** in cNEO-DFT at each proton expectation position is plotted in (c). The **f** vectors correspond to the negative of the energy gradient in (a) and serve as the force acting on the proton at each expectation position.

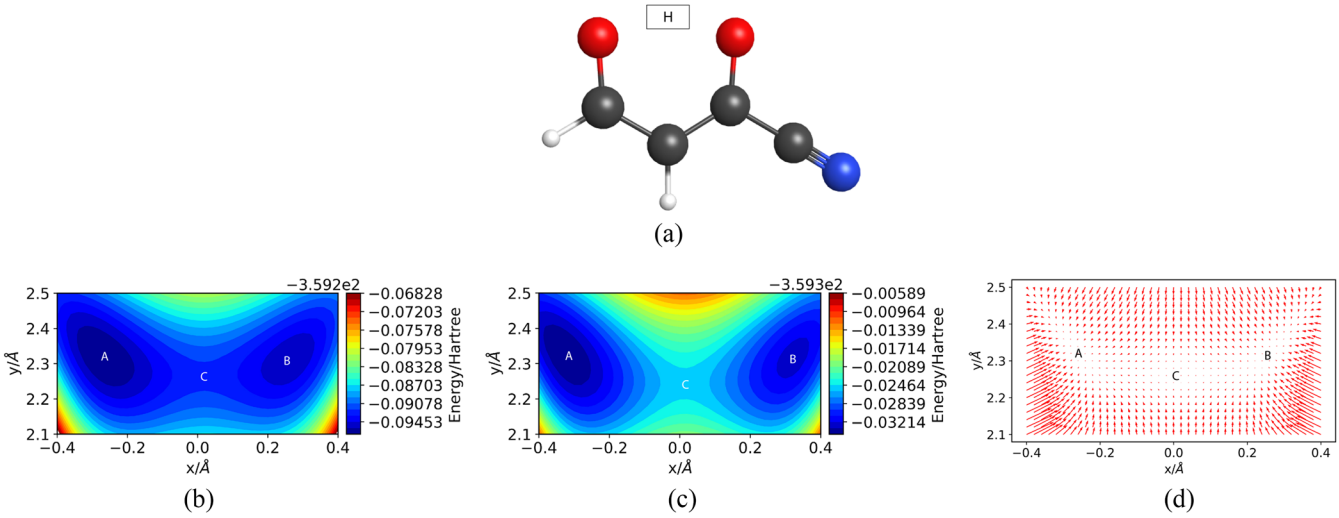

FIG. 4. Structure of the 2-cyano-malonaldehyde molecule (a) with the hydrogen transfer region highlighted in a box. Energy surfaces for the hydrogen transfer calculated by cNEO-DFT and DFT are plotted in (b) and (c), respectively. All classical nuclei are in the x–y plane and fixed at an average reactant/product geometry. The proton expectation positions are constrained to different points closed to the two equilibrium positions in the x-y plane. The coordinates (in Å) of the two nearby O atoms are (1.284, 1.973) and (−1.275, 1.972), respectively. Although the absolute energies are different, the energy intervals in the plots are set to be the same to facilitate the comparison. The Lagrange multiplier **f** in cNEO-DFT at each proton expectation position is plotted in (d), and the vector field corresponds to the negative of the energy gradient in (b).

located.[19] They correspond to the species with the hydrogen atom attached to the left and right oxygen, respectively. Here, using the cNEO-DFT method, not only the two local minima, but also the saddle point can be identified. These stationary points are labeled with A, B, and C in Fig. 4(b). They are also characterized by vanishing force vectors **f** in Fig. 4(d). Compared with the conventional DFT results in Fig. 4(c), the geometries of the transition state are similar, whereas the two local minima by cNEO-DFT in Fig. 4(b) are closer to each other. In addition, cNEO-DFT predicts a much lower barrier height for the proton transfer between the two nearby oxygen atoms. Previously, it has been shown that *ab initio* molecular dynamics calculations based on the DFT potential energy surface significantly overestimate the free-energy barrier for the hydrogen transfer in malonaldehyde.[37] Our cNEO-DFT with a lower energy barrier may potentially provide a viable solution to this challenging problem.

V. CONCLUSIONS

In this paper, we developed cNEO-DFT starting from a constraint on the expectation value of the position for the quantum nucleus. This constraint is introduced through the Lagrange multiplier method. When the Lagrangian function is stationary with respect to the variation of orbitals as well as the change of the Lagrange multiplier, solutions can be obtained, which contains information on the orbitals, orbital energies, and the force applied on the quantum nucleus. The cNEO method extends the NEO energy surface by including the expectation position of the quantum nuclei as a variable, and nuclear quantum effects due to the delocalized nuclear density can be incorporated on the whole energy surface. Calculations on the three test systems showed the notable influence of the proton quantum effects on the energy landscape. In particular, at the transition state for a hydrogen transfer system, the barrier is lower and the geometry is slightly different from that obtained from conventional DFT. Therefore, the cNEO method, which naturally includes nuclear quantum effects, can be potentially used in geometry optimization, transition states search, and dynamics calculations. In principle, the constraint on the expectation position can be applied to any number of quantum particles. Consequently, without invoking the Born–Oppenheimer approximation, cNEO-DFT can also potentially describe all electrons and nuclei in a molecule quantum-mechanically, which may make it an alternative way to the exact factorization method.[38–40] This theoretical formulation of cNEO-DFT opens up new directions for future method developments and practical applications.

SUPPLEMENTARY MATERIAL

See the supplementary material for the coordinates of the fixed classical nuclei in the three test systems: FHF^-, HCN/HNC isomerization, and hydrogen transfer in 2-cyano-malondialdehyde.

ACKNOWLEDGMENTS

We are grateful for the support and funding from the University of Wisconsin via the Wisconsin Alumni Research Foundation.

APPENDIX: PROOF: LAGRANGE MULTIPLIER IS THE FORCE ACTING ON THE PROTON

For each proton expectation position $\mathbf{R}_0$, the proper **f** is a function of $\mathbf{R}_0$ and can be solved using the method discussed in Sec. II,

$$\mathbf{f} = \mathbf{f}(\mathbf{R}_0). \tag{A1}$$

Consequently, from Eq. (13), the electron and proton orbitals are also determined by the proton expectation position $\mathbf{R}_0$,

$$\phi = \phi(\mathbf{f}(\mathbf{R}_0)). \tag{A2}$$

From Eqs. (2) to (4), the total energy E only explicitly depends on ϕ. Then, the chain rule can be used to calculate the derivative of the energy E with respect to $\mathbf{R_0}$,

$$\begin{aligned}
\frac{\mathrm{d}E(\mathbf{R}_0)}{\mathrm{d}\mathbf{R}_0} &= \sum_{\phi} \int \frac{\delta E}{\delta \phi^*(\mathbf{r})} \frac{\mathrm{d}\phi^*(\mathbf{r})}{\mathrm{d}\mathbf{f}} \frac{\mathrm{d}\mathbf{f}}{\mathrm{d}\mathbf{R}_0} \mathrm{d}\mathbf{r} + \text{c.c.} \\
&= \sum_{\phi} \int \frac{\delta\left(L - \mathbf{f}\cdot\left(\langle\phi^p|\mathbf{r}|\phi^p\rangle - \mathbf{R}_0\right) + \sum_i \epsilon_i^e\left(\langle\phi_i^e|\phi_i^e\rangle - 1\right) + \epsilon^p\left(\langle\phi^p|\phi^p\rangle - 1\right)\right)}{\delta\phi^*(\mathbf{r})} \frac{\mathrm{d}\phi^*(\mathbf{r})}{\mathrm{d}\mathbf{f}} \frac{\mathrm{d}\mathbf{f}}{\mathrm{d}\mathbf{R}_0} \mathrm{d}\mathbf{r} + \text{c.c.} \\
&= -\int \mathbf{f}\cdot\mathbf{r}\phi^p(\mathbf{r}) \frac{\mathrm{d}\phi^{p*}(\mathbf{r})}{\mathrm{d}\mathbf{f}} \frac{\mathrm{d}\mathbf{f}}{\mathrm{d}\mathbf{R}_0} \mathrm{d}\mathbf{r} + \text{c.c.} \\
&= -\mathbf{f}\cdot\frac{\mathrm{d}\langle\phi^p|\mathbf{r}|\phi^p\rangle}{\mathrm{d}\mathbf{f}} \frac{\mathrm{d}\mathbf{f}}{\mathrm{d}\mathbf{R}_0} \\
&= -\mathbf{f}\cdot\frac{\mathrm{d}\mathbf{R}_0}{\mathrm{d}\mathbf{f}} \frac{\mathrm{d}\mathbf{f}}{\mathrm{d}\mathbf{R}_0} \\
&= -\mathbf{f},
\end{aligned} \tag{A3}$$

where c.c. denotes the complex conjugate. Note that in the derivation above, we have used the conclusion in Eq. (15), and the orbital derivative for the normalization constraint term is zero because

$$\begin{aligned}
\int \frac{\delta\epsilon_i\left(\langle\phi_i|\phi_i\rangle - 1\right)}{\delta\phi_i^*(\mathbf{r})} \frac{\mathrm{d}\phi_i^*(\mathbf{r})}{\mathrm{d}\mathbf{f}} \frac{\mathrm{d}\mathbf{f}}{\mathrm{d}\mathbf{R}_0} \mathrm{d}\mathbf{r} + \int \frac{\delta\epsilon_i\left(\langle\phi_i|\phi_i\rangle - 1\right)}{\delta\phi_i(\mathbf{r})} \frac{\mathrm{d}\phi_i(\mathbf{r})}{\mathrm{d}\mathbf{f}} \frac{\mathrm{d}\mathbf{f}}{\mathrm{d}\mathbf{R}_0} \mathrm{d}\mathbf{r} &= \int \epsilon_i\phi_i(\mathbf{r}) \frac{\mathrm{d}\phi_i^*(\mathbf{r})}{\mathrm{d}\mathbf{f}} \frac{\mathrm{d}\mathbf{f}}{\mathrm{d}\mathbf{R}_0} \mathrm{d}\mathbf{r} + \int \epsilon_i\phi_i^*(\mathbf{r}) \frac{\mathrm{d}\phi_i(\mathbf{r})}{\mathrm{d}\mathbf{f}} \frac{\mathrm{d}\mathbf{f}}{\mathrm{d}\mathbf{R}_0} \mathrm{d}\mathbf{r} \\
&= \frac{\epsilon_i \mathrm{d}\langle\phi_i|\phi_i\rangle}{\mathrm{d}\mathbf{f}} \frac{\mathrm{d}\mathbf{f}}{\mathrm{d}\mathbf{R}_0} = 0.
\end{aligned} \tag{A4}$$

Alternatively, the same conclusion can be drawn from a different proof as follows:

When minimization of the Lagrangian function is achieved with the constraints satisfied, we have

$$\frac{\delta L(\phi, \mathbf{f}, \mathbf{R}_0)}{\delta\phi}\Big|_{\mathbf{f},\mathbf{R}_0} = 0 \tag{A5}$$

and

$$\frac{\partial L(\phi, \mathbf{f}, \mathbf{R}_0)}{\partial\mathbf{f}}\Big|_{\phi,\mathbf{R}_0} = \langle\phi^p|\mathbf{r}|\phi^p\rangle - \mathbf{R_0} = 0. \tag{A6}$$

Then, the total energy E equals the Lagrangian function L, and

$$\begin{aligned}
\frac{\mathrm{d}E(\mathbf{R}_0)}{\mathrm{d}\mathbf{R}_0} &= \frac{\mathrm{d}L(\phi(\mathbf{f}(\mathbf{R}_0)), \mathbf{f}(\mathbf{R}_0), \mathbf{R}_0)}{\mathrm{d}\mathbf{R}_0} \\
&= \sum_{\phi} \int \frac{\delta L}{\delta\phi} \frac{\mathrm{d}\phi}{\mathrm{d}\mathbf{f}} \frac{\mathrm{d}\mathbf{f}}{\mathrm{d}\mathbf{R}_0} \mathrm{d}\mathbf{r} + \frac{\partial L}{\partial\mathbf{f}} \frac{\mathrm{d}\mathbf{f}}{\mathrm{d}\mathbf{R}_0} + \frac{\partial L}{\partial\mathbf{R}_0} \\
&= 0 + 0 + \frac{\partial L}{\partial\mathbf{R}_0} \\
&= -\mathbf{f}.
\end{aligned} \tag{A7}$$

The result in Eqs. (A3) and (A7) indicates that $\mathbf{f}$ is the negative gradient of the energy with respect to the expectation value of the proton position $\mathbf{R}_0$. In other words, $\mathbf{f}$ is the force acting on the quantum nucleus when the nucleus is at the expectation position $\mathbf{R}_0$.

REFERENCES

[1] S. Hammes-Schiffer, J. Am. Chem. Soc. **137**, 8860 (2015).
[2] C. Liu, B. C. Colón, M. Ziesack, P. A. Silver, and D. G. Nocera, Science **352**, 1210 (2016).
[3] W. J. Youngblood, S.-H. A. Lee, Y. Kobayashi, E. A. Hernandez-Pagan, P. G. Hoertz, T. A. Moore, A. L. Moore, D. Gust, and T. E. Mallouk, J. Am. Chem. Soc. **131**, 926 (2009).
[4] M. L. Helm, M. P. Stewart, R. M. Bullock, M. R. DuBois, and D. L. DuBois, Science **333**, 863 (2011).
[5] T. J. Meyer, M. H. V. Huynh, and H. H. Thorp, Angew. Chem., Int. Ed. **46**, 5284 (2007).
[6] V. R. I. Kaila, M. I. Verkhovsky, and M. Wikström, Chem. Rev. **110**, 7062 (2010).
[7] S. P. Webb, T. Iordanov, and S. Hammes-Schiffer, J. Chem. Phys. **117**, 4106 (2002).
[8] H. Nakai, Int. J. Quantum Chem. **107**, 2849 (2007).
[9] M. V. Pak, A. Chakraborty, and S. Hammes-Schiffer, J. Phys. Chem. A **111**, 4522 (2007).
[10] T. Ishimoto, M. Tachikawa, and U. Nagashima, Int. J. Quantum Chem. **109**, 2677 (2009).
[11] F. Pavošević, T. Culpitt, and S. Hammes-Schiffer, J. Chem. Theory Comput. **15**, 338 (2019).
[12] F. Pavošević and S. Hammes-Schiffer, J. Chem. Phys. **151**, 074104 (2019).
[13] A. Chakraborty, M. V. Pak, and S. Hammes-Schiffer, Phys. Rev. Lett. **101**, 153001 (2008).

[14]T. Udagawa, T. Tsuneda, and M. Tachikawa, Phys. Rev. A **89**, 052519 (2014).
[15]A. Sirjoosingh, M. V. Pak, K. R. Brorsen, and S. Hammes-Schiffer, J. Chem. Phys. **142**, 214107 (2015).
[16]Y. Yang, K. R. Brorsen, T. Culpitt, M. V. Pak, and S. Hammes-Schiffer, J. Chem. Phys. **147**, 114113 (2017).
[17]K. R. Brorsen, P. E. Schneider, and S. Hammes-Schiffer, J. Chem. Phys. **149**, 044110 (2018).
[18]K. R. Brorsen, Y. Yang, and S. Hammes-Schiffer, J. Phys. Chem. Lett. **8**, 3488 (2017).
[19]Y. Yang, T. Culpitt, Z. Tao, and S. Hammes-Schiffer, J. Chem. Phys. **149**, 084105 (2018).
[20]Y. Yang, T. Culpitt, and S. Hammes-Schiffer, J. Phys. Chem. Lett. **9**, 1765 (2018).
[21]Y. Yang, P. E. Schneider, T. Culpitt, F. Pavošević, and S. Hammes-Schiffer, J. Phys. Chem. Lett. **10**, 1167 (2019).
[22]T. Culpitt, Y. Yang, F. Pavošević, Z. Tao, and S. Hammes-Schiffer, J. Chem. Phys. **150**, 201101 (2019).
[23]T. Iordanov and S. Hammes-Schiffer, J. Chem. Phys. **118**, 9489 (2003).
[24]A. D. Bochevarov, E. F. Valeev, and C. David Sherill, Mol. Phys. **102**, 111 (2004).
[25]Q. Wu and T. Van Voorhis, Phys. Rev. A **72**, 024502 (2005).
[26]Q. Wu and T. Van Voorhis, J. Chem. Theory Comput. **2**, 765 (2006).
[27]P. Ramos and M. Pavanello, J. Chem. Phys. **148**, 144103 (2018).
[28]D. A. Knoll and D. E. Keyes, J. Comput. Phys. **193**, 357 (2004).
[29]V. Eyert, J. Comput. Phys. **124**, 271 (1996).
[30]D. D. O'Regan and G. Teobaldi, Phys. Rev. B **94**, 035159 (2016).
[31]Q. Sun, T. C. Berkelbach, N. S. Blunt, G. H. Booth, S. Guo, Z. Li, J. Liu, J. D. McClain, E. R. Sayfutyarova, S. Sharma, S. Wouters, and G. K.-L. Chan, WIREs Comput. Mol. Sci. **8**, e1340 (2018).
[32]A. D. Becke, Phys. Rev. A **38**, 3098 (1988).
[33]C. Lee, W. Yang, and R. G. Parr, Phys. Rev. B **37**, 785 (1988).
[34]A. D. Becke, J. Chem. Phys. **98**, 5648 (1993).
[35]T. H. Dunning, J. Chem. Phys. **90**, 1007 (1989).
[36]R. D. Bardo and K. Ruedenberg, J. Chem. Phys. **60**, 918 (1974).
[37]M. E. Tuckerman and D. Marx, Phys. Rev. Lett. **86**, 4946 (2001).
[38]A. Abedi, N. T. Maitra, and E. K. U. Gross, Phys. Rev. Lett. **105**, 123002 (2010).
[39]A. Abedi, N. T. Maitra, and E. Gross, J. Chem. Phys. **137**, 22A530 (2012).
[40]L. Lacombe, N. M. Hoffmann, and N. T. Maitra, Phys. Rev. Lett. **123**, 083201 (2019).